Optimal design and operation of a syngas-fuelled SOFC micro CHP system for residential applications in different climate zones in China

Yang, Wenyuan; Zhao, Yingru; Liso, Vincenzo; Brandon, Nigel

Published in:
Energy and Buildings

DOI (link to publication from Publisher):
10.1016/j.enbuild.2014.05.015

Publication date:
2014

Document Version
Early version, also known as pre-print

Energy and Buildings 80 (2014) 613–622

Contents lists available at ScienceDirect

Energy and Buildings

journal homepage: www.elsevier.com/locate/enbuild

Optimal design and operation of a syngas-fuelled SOFC micro-CHP system for residential applications in different climate zones in China

Wenyuan Yang [a], Yingru Zhao [a,*], Vincenzo Liso [b], Nigel Brandon [c]

[a] School of Energy Research, Xiamen University, Xiamen, China
[b] Department of Energy Technology, Aalborg University, Aalborg, Denmark
[c] Earth Science and Engineering, Imperial College London, London, UK

ARTICLE INFO

Article history:
Available online 23 May 2014

Keywords:
Syngas-fuelled SOFC
Residential micro-CHP system
Optimal design and operation
Different climate zone

ABSTRACT

Fuel cell based micro-CHP systems are expected to be one of the most promising technologies for implementation in the residential sector. Since the design and operation of such CHP systems are greatly dependent upon the seasonal atmospheric conditions, it is important to evaluate their performance under difference climate conditions to ensure that it is well matched with the local heat-to-power ratio. The aim of this study is to investigate the optimal design and operation of a syngas-fuelled SOFC micro-CHP system for small households located in five different climate zones in China. The ability of the micro-CHP to cover the heat and electricity demand of a 70 m^2 single-family apartment with an average number of occupants of 3 is evaluated. A detailed model of the micro-CHP unit coupled with a hot water storage tank and an auxiliary boiler is developed. System design trade-offs are discussed to determine the optimal match between the energy demand of the household for different climates across China and the energy supply of the micro-CHP during the whole year. Moreover, criteria for sizing the system components of the micro-CHP are specifically addressed. The developed methodology can be applied to different types of residence with different load profiles.

1. Introduction

Energy technologies with high efficiency and low environmental impact are urgently needed to overcome the threats posed by climate change and energy security. In the residential sector, energy consumption can be considerably reduced by enhancing the efficiency of energy supply. Fuel cell technologies are suitable for domestic micro-generation to meet the basic energy supply requirements for a single-family apartment. They can be easily integrated into existing heating system, and as such they are increasingly finding application in the residential sector extensively due to their favourable characteristics under a regime of pollution reducing policies and deregulation of the electricity market [1]. Specifically, micro-cogeneration systems (micro-CHP) based on fuel cells [2,3] represent an interesting alternative to traditional CHP technologies [4] to efficiently meet the heating and electricity needs of residential dwellings.

Among the various fuel cell CHP systems, micro-CHP based on Solid Oxide Fuel Cells (SOFCs) is potentially attractive due to its ability to operate at high efficiency on commonly available hydrocarbon fuels such as natural gas or syngas [5–8]. Many research works concerning the performance evaluation and design analysis of SOFC CHP systems [9,10] have been presented in the technical literature, indicating the growing interest in determining and demonstrating its potential for high-efficiency buildings. At the same time, some studies [11] have produced economic investigation and assessment of these systems for different building configurations [10,12], showing that this type of technology can reduce significantly the energy consumption and costs of commercial or residential buildings.

Depending on the degree of electrical and thermal interconnection to the wider energy network, it can be important to match the energy generated by the micro-CHP system with the instantaneous electricity and heat demand of a residential apartment. A typical apartment has a relatively low-level of energy consumption for the majority of the day with electrical requirements reaching several kilowatts when high power devices are operated, and even higher heating loads when space heating is required. An SOFC micro-CHP unit therefore needs to generate not only heat to support the space and water heating but also electrical power for lightning and other appliances. Furthermore, continuous operation can reduce degradation arising from thermal cycling and the associated mechanical

* Corresponding author. Tel.: +86 592 5952781; fax: +86 592 2188053.
E-mail address: yrzhao@xmu.edu.cn (Y. Zhao).

http://dx.doi.org/10.1016/j.enbuild.2014.05.015
0378-7788/

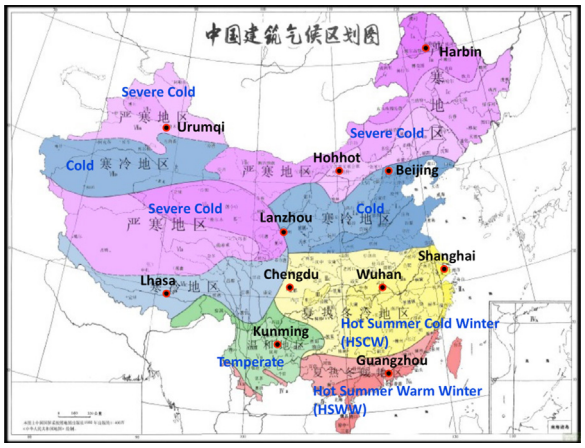

Fig. 1. Map of building climate zones in China.

stresses. There is thus a link between the operating strategy and the heat storage capacity. Although the heat-to-power ratio of a micro-CHP system can be varied when operating at different electrical loads, and through use of an auxiliary burner, there are bounds on the range of heat-to-power ratio that can be achieved [7,13].

Moreover, the design and operation of CHP systems are greatly dependent upon seasonal atmospheric conditions, which determine directly the thermal and electrical demands of residents. It is therefore important to evaluate the performance of the CHP system under difference climate conditions to ensure that it matches well with the local heat-to-power ratio [7]. A few studies have simulated the performance of micro-CHP systems in a domestic environment, responding to the patterns of energy demand from a typical family [7,11,14–17]. However, energy consumption tends to be quite different in every country, so demand profiles are not easily transferred from other countries' building stock.

This study aims to investigate the optimal design and operation of a syngas-fuelled SOFC micro-CHP system for small apartments located in five different climate zones in China. The ability of the micro-CHP to cover the heat and electricity demand of a 70 m^2 single-family household with an average number of occupants of 3 is evaluated. System design trade-offs and optimal operating strategies are addressed specifically. The proposed methodology can be applied to different types of residence with different load profiles, providing a target driven solution that evaluates and optimizes the decision process to enhance building energy efficiency in China.

2. Climate regions and energy demand profile in China

The climate across China varies considerably and the country can be divided into several climate zones, which are mainly Severe Cold, Cold, Hot Summer Cold Winter (HSCW), Hot Summer Warm Winter (HSWW) and Temperate [18], as shown in Fig. 1.

In the present study, five cities have been chosen as representatives from five different climate zones for the analysis of the micro-CHP system as listed in Table 1 [18–23], where HDD18 is the number of heating days in a whole year when the daily average outdoor temperature is below 18 °C, and CDD26 is the number of cooling days in a whole year when the daily average outdoor temperature is above 26 °C. Based on the Human-earth System Database [24], the annul temperature profiles of five representative cities are plotted in Fig. 2.

The micro-CHP system has the potential to substitute the natural gas boiler used in many single family households, with the additional capacity to produce electricity. In the present study, we have considered a single-family apartment with 70 m^2 heated area and an average number of occupants of 3. The energy demand for

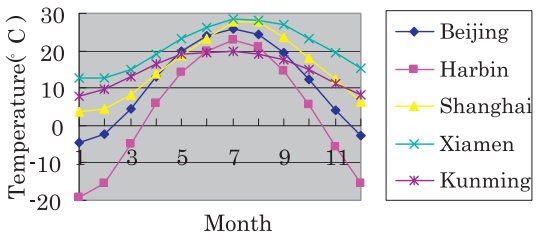

Fig. 2. Annul temperature profile of five representative cities.

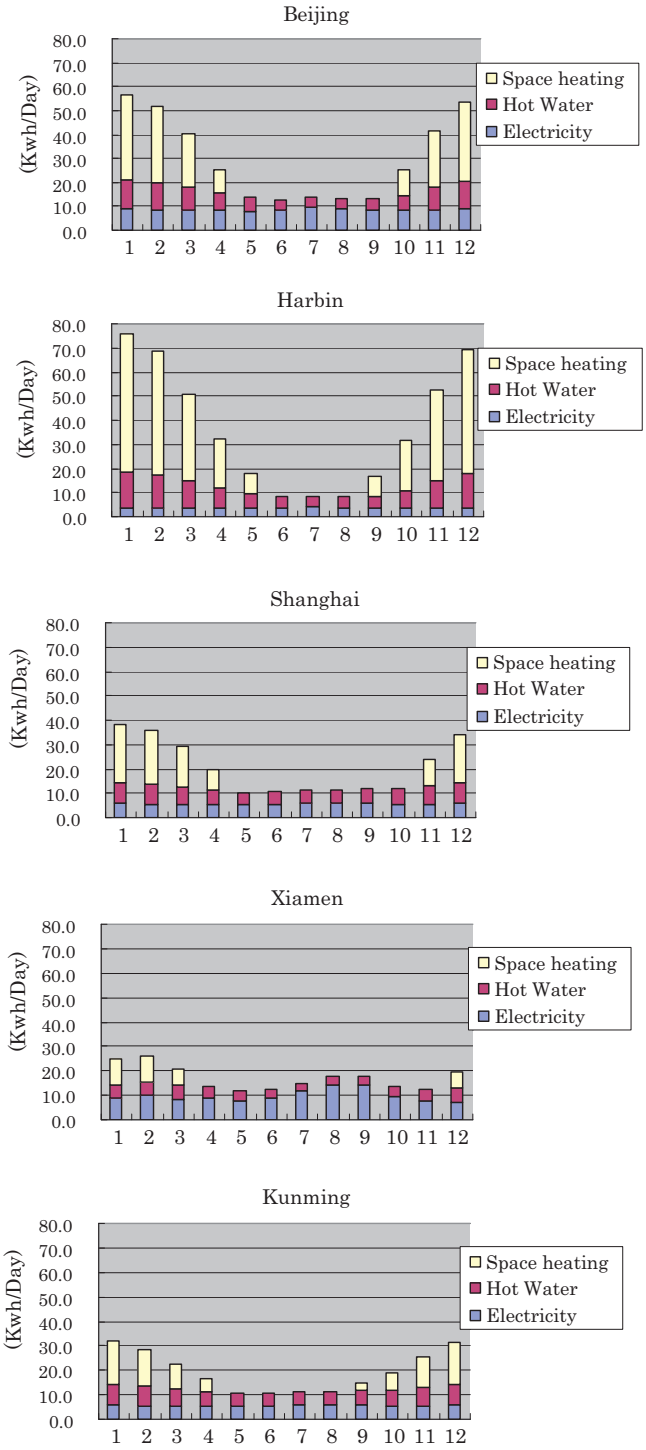

Fig. 3. Residential energy demand profile for a 70 m^2 single-family household in five representative cities.

Table 1
Energy demand profile of the representative cities [18–23].

No.	Climate zone	Representative city	Climate condition
I	Severe Cold	Harbin	$3800 \leq HDD18 < 8000$
II	Cold	Beijing	$2000 \leq HDD18 < 3800$, $CDD26 \leq 200$
III	Hot Summer Cold Winter	Shanghai	$600 \leq HDD18 < 2000$, $50 < CDD26 \leq 300$
IV	Hot Summer Warm Winter	Xiamen	$HDD18 < 600$, $CDD26 > 200$
V	Temperate	Kunming	$HDD18 < 2000$, $CDD26 \leq 50$

space heating are calculated with Tangent heating and ventilation calculating software [25], where the thermal environment design index for indoor space heating at winter are as follows:

- Indoor design temperature for bedroom and living room is 18 °C.
- Ventilation frequency is 0.5 times/h.

Energy demand for residential hot water and electricity are calculated with data from [26,27]. Fig. 3 illustrates the energy demand for residential space heating, hot water and electricity over a year for the single-family apartment with 70 m^2 heated area in five different representative cities. As shown in Fig. 3, the energy demand of electricity and hot water do not vary much over the year, whereas the demand for space heating varies significantly in different months, no matter which region the household is located in. Space heating demand is by far the most sensitive data as it varies dramatically with the building structure, heat-insulation properties and family living standards. The annual space heating demand is around 8700 kWh in Harbin, 5000 kWh in Beijing, 3050 kWh in Shanghai, 2600 kWh in Kunming and 1050 kWh in Xiamen, respectively.

3. System configuration and model assumptions

3.1. System configuration

The schematic diagram of the micro-CHP system is depicted in Fig. 4, where the SOFC is fuelled with syngas and coupled with a hot water tank as a heat store. Air is supplied by a blower and preheated prior to entry to the SOFC. The product gas of the SOFC is sent into an afterburner, where the un-reacted fuel is burnt with part of the excess air. Upstream of the fuel cell, two heat exchangers (HEX1 and HEX2) are adopted to serve as pre-heaters, recovering heat from the exhaust gas of the afterburner for preheating the inlet air and fuel before they enter the fuel cell. A hot water storage tank is used to incorporate with the fuel cell unit in order to supply hot water for the apartment with the residual heat of the exhaust gas, while extra heat can be obtained from an auxiliary boiler to cover the additional heat demand. This enables the heat-to-power ratio of the CHP system to be varied, allowing the system to cover a greater portion of domestic thermal energy demand in cold seasons.

3.2. Model assumptions

A number of simplifications and assumptions were made when developing the model of the electrochemical and thermodynamic characteristics of the CHP system:

- The fuel cell is assumed to be operated under steady-state conditions.
- The fuel cell reactions are assumed to be in equilibrium.
- Syngas consists of the following gas species, $j = \{H_2, CO, CH_4, CO_2, H_2O, N_2\}$.
- Air that enters the fuel cell consists of 79% N_2 and 21% O_2.
- The cathode and anode inlet temperature of the fuel cell are assumed to be equal.
- The cathode and anode exit temperature of the fuel cell are assumed to be equal.
- There is a temperature gradient (ΔT) across the fuel cell. The temperature of the solid structure (T) is homogeneous and midway between the inlet and exit temperatures.
- All gases behave as ideal gases.
- Gas leakage is negligible.
- Heat loss to the environment occurs only in the fuel cell.

With the help of these assumptions, a model of the micro-CHP system has been constructed and the governing equations representing all modelled components are given in the following sections. Each of the system components are modelled individually and integrated to form the overall micro-CHP system.

4. Modelling of the micro-CHP system

4.1. Modelling the solid oxide fuel cell fuelled with coal syngas

SOFCs are devices for the electrochemical conversion of a fuel gas into electrical energy. Various fuel options are feasible for SOFC operation, while coal derived syngas represents a more economical

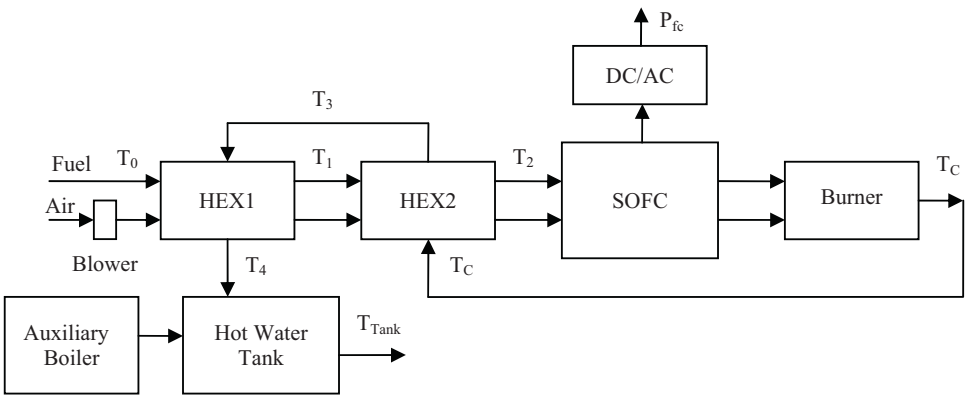

Fig. 4. The schematic diagram of the micro-CHP system.

option given the abundance of the fuel as well as the development of gasification technology in China. The coal syngas consists primarily of hydrogen and CO, with significant water vapour and some levels of CO_2 and other minority species [28].

As commonly assumed, only H_2 oxidation is considered to contribute to electrochemical power generation, while CH_4 is reformed to CO, which is then converted to CO_2 and H_2 through the water-gas shift reaction [29–31]. Consequently, the steam reforming reaction for methane, the water-gas shift reaction, and the electrochemical reactions occur simultaneously in the SOFC are summarized as follows:

$$CH_4 + H_2O \rightarrow CO + 3H_2 \text{ (steamreforming)} \quad (1)$$

$$CO + H_2O \rightarrow CO_2 + H_2 \text{ (water gas shift)} \quad (2)$$

$$H_2 + \tfrac{1}{2}O_2 \rightarrow H_2O \text{ (overall cell reaction)} \quad (3)$$

A single cell model is taken to be representative of the SOFC, which accounts for internal reforming and water-gas shift equilibrium, electrochemical polarizations and the associated heat generation, mass transfer via cell reactions, and overall energy balances. This representation can be readily constructed as quantities such as stack voltage and stack power which are scaled versions of single-cell voltage and power.

4.1.1. Mass balance

The amount of hydrogen consumed in the fuel cell reactions, $\dot{n}_{H_{2-c}}$ (mol s^{-1}), is related to the current by Faraday's law:

$$\dot{n}_{H_{2-c}} = \frac{iA}{n_e F} \quad (4)$$

where i denotes the current density, A represents the surface area of the interconnect plate (assuming the interconnect plates all have the same area), n_e is the number of electrons transferred per mole of reactant, and $F = 96{,}485$ C mol^{-1} is Faraday's constant. For a known fuel utilization factor, U_f, the amount of hydrogen supplied, $\dot{n}_{H_{2-s}}$ (mol s^{-1}), is given by

$$\dot{n}_{H_{2-s}} = \frac{\dot{n}_{H_{2-c}}}{U_f} = \frac{iA}{n_e F U_f} \quad (5)$$

The molar flow rate of the fuel stream needed to produce the required amount of hydrogen $\dot{n}_{f-in}$ (mol s^{-1}) is thus

$$\dot{n}_{f-in} = \frac{\dot{n}_{H_{2-s}}}{x_{fc}} = \frac{iA}{n_e F U_f x_{fc}} \quad (6)$$

where x_{fc} is the number of moles of hydrogen produced by 1 mol of fuel, which can be calculated according to the composition of the fuel as $x_{fc} = x_{H_2} + x_{CO} + 4x_{CH_4}$. For a known fuel gas composition x_j, the molar flow rate for each component j in the fuel stream is:

$$\dot{n}_{f-in}(j) = \dot{n}_{f-in} x_j = \frac{iAx_j}{n_e F U_f x_{fc}} \quad (7)$$

where $j = \{H_2, CO, CH_4, CO_2, H_2O, N_2\}$.

In order to avoid carbon deposition, an amount of steam equivalent to twice the amount needed for the reforming and water-gas shift reactions is supplied. The molar flow rate of steam needed, $\dot{n}_{H_2O}$ (mol s^{-1}) is thus

$$\dot{n}_{H_2O} = (\dot{n}_{f-in}(CO) + \dot{n}_{f-in}(CH_4) \times 2) \times 2 \quad (8)$$

The molar flow rate of additional steam supplied is thus given by

$$\begin{aligned}\dot{n}_{ADD} &= \dot{n}_{H_2O} - \dot{n}_{f-in}(H_2O) \\ &= \dot{n}_{H_2O} = (\dot{n}_{f-in}(CO) + \dot{n}_{f-in}(CH_4) \times 2) \times 2 - \dot{n}_{f-in}(H_2O)\end{aligned} \quad (9)$$

Therefore the total molar flow rate of the fuel stream entering the fuel cell, $\dot{n}_f$ (mol s^{-1}) becomes

$$\dot{n}_f = \dot{n}_{f-in} + \dot{n}_{ADD} \quad (10)$$

For known conversions of the reforming and water gas shift reactions, the component flow rates in the fuel exit stream are given as

$$\dot{n}_{f-out}(H_2) = \dot{n}_{H_{2-S}} \times (1 - U_f) \quad (11)$$

$$\dot{n}_{f-out}(CO) = 0 \quad (12)$$

$$\dot{n}_{f-out}(CO_2) = \dot{n}_{f-in}(CO) + \dot{n}_{f-in}(CO_2) + \dot{n}_{f-in}(CH_4) \quad (13)$$

$$\dot{n}_{f-out}(CH_4) = 0 \quad (14)$$

$$\dot{n}_{f-out}(H_2O) = \frac{\dot{n}_{H_2O}}{2} + \dot{n}_{H_{2-S}} \times U_f \quad (15)$$

$$\dot{n}_{f-out}(N_2) = \dot{n}_{f-in}(N_2) \quad (16)$$

Given a known inlet composition, the molar flow rates for the air stream are:

$$\dot{n}_{a-in}(O_2) = \dot{n}_{H_{2-s}} \times \frac{U_f/2}{U_a} \quad (17)$$

$$\dot{n}_{a-in}(N_2) = \dot{n}_{a-in}(O_2)\frac{0.79}{0.21} \quad (18)$$

$$\dot{n}_{a-out}(O_2) = \dot{n}_{a-in}(O_2) \times (1 - U_a) \quad (19)$$

$$\dot{n}_{a-out}(N_2) = \dot{n}_{a-in}(N_2) \quad (20)$$

where U_a is the air utilization factor, the subscript '*f*' refers to the fuel stream, the subscript '*a*' to the air stream, the subscript '*in*' to the fuel cell inlet and the subscript '*out*' the fuel cell outlet.

4.1.2. Electrochemical descriptions

The theoretical open-circuit voltage of an SOFC can be determined by the Nernst equation given as follows [32–35]:

$$E = \frac{-\Delta g(T,P)}{n_e F} \quad (21)$$

Note that the molar Gibbs free energy change for the SOFC reaction depends dramatically on the temperature (T) and partial pressures of reactants (p), i.e., $\Delta g(T,P) = \Delta g^\circ(T) - RT\ln(p_{H_2} p_{O_2}^{1/2})$, where $R = 8.314$ J mol^{-1} K^{-1} is the universal gas constant, $\Delta g^\circ(T) = \Delta h^\circ - T\Delta s^\circ$ stands for the molar Gibbs free energy change at $p_0 = 1$ atm which also depends on temperature [32–34,36], p_{H_2}, p_{O_2} and p_{H_2O} are the partial pressures of reactants H_2, O_2, and H_2O, respectively.

The Nernst potential is the maximum reversible voltage of an SOFC at given conditions, however the voltage of an operating SOFC is generally lower than this. As current is drawn from the fuel cell, the voltage falls due to internal resistances and overpotential losses. These losses are common to all types of fuel cells and cannot be eliminated [31,32,34]. Therefore, three types of polarizations, i.e., activation, ohmic and concentration, are considered and calculated through Eqs. (22)–(30).

(1) *Activation overpotential* depends on the kinetics of the electrochemical reactions occurring at the anode and cathode. According to the general Butler–Volmer equation, the respective activation overpotentials of the anode and cathode can be calculated as

$$V_{act,a} = \frac{2RT}{n_e F}\sinh^{-1}\left(\frac{i}{2i_{0,a}}\right) \quad (22)$$

$$V_{act,a} = \frac{2RT}{n_e F}\sinh^{-1}\left(\frac{i}{2i_{0,c}}\right) \quad (23)$$

Table 2
Operating conditions and major parameters [6,29,32].

Parameter	Symbol	Value
Ambient temperature (K)	T_0	298
Operating pressure (atm)	p_0	1
Fuel utilization	U_f	0.8
Air utilization	U_a	0.2
Number of electrons	n_e	2
Anode exchange current density ($A\,m^{-2}$)	$i_{0,a}$	6500
Cathode exchange current density ($A\,m^{-2}$)	$i_{0,c}$	2500
Limiting current density ($A\,m^{-2}$)	i_L	9000
Anode thickness (μm)	L_a	500
Anode conductivity constants	C_{1a}; C_{2a}	95×10^6; −1150
Cathode thickness (μm)	L_c	50
Cathode conductivity constants	C_{1c}; C_{2c}	42×10^6; −1200
Electrolyte thickness (μm)	L_e	10
Electrolyte conductivity constants	C_{1e}; C_{2e}	3.34×10^4; −10,300
Interconnect thickness (cm)	L_{int}	0.3
Interconnect conductivity constants	C_{1int}; C_{2int}	9.3×10^6; −1100
Air blower power consumption factor	η_{ab}	10%

where $i_{0,a/c}$ denotes the anode/cathode exchange current density.

(2) *Ohmic overpotential* is caused mostly by resistance to the conduction of ions and electrons, and by contact resistance between the fuel cell components. In the present study, Ohmic losses are simulated as follows assuming a series electrical scheme:

$$V_{ohm} = I\sum R_k = iA\sum \frac{L_k}{\sigma_k A} = i\sum \frac{L_k}{\sigma_k} = i\left(\frac{L_e}{\sigma_e}+\frac{L_a}{\sigma_a}+\frac{L_c}{\sigma_c}+\frac{L_{\text{int}}}{\sigma_{\text{int}}}\right) \quad (24)$$

$$\sigma_e = C_{1e}\exp(C_{2e}) \quad (25)$$

$$\sigma_a = \frac{C_{1a}}{T}\exp\left(\frac{C_{2a}}{T}\right) \quad (26)$$

$$\sigma_c = \frac{C_{1c}}{T}\exp\left(\frac{C_{2c}}{T}\right) \quad (27)$$

$$\sigma_{\text{int}} = \frac{C_{\text{int}}}{T}\exp\left(\frac{C_{\text{int}}}{T}\right) \quad (28)$$

where R_k represents the resistance, L_k is the thickness, A is the area, and σ_k denotes the electronic conductivity of the anode, cathode, interconnect and the ionic conductivity of the electrolyte. $C_{1ent}-C_{int}$ are constants listed in Table 2. The subscripts *a*, *c*, *e* and *int* denote anode, cathode, electrolyte and interconnect, respectively.

(3) *Concentration overpotential* is the voltage drop due to mass transfer limitations from the gas phase into and through the electrode. In the present study, the calculation of concentration overvoltage is as follows:

$$V_{conc,a} = \frac{RT}{n_eF}\ln\left(1-\frac{i}{2i_{L,a}}\right) \quad (29)$$

$$V_{conc,c} = \frac{RT}{n_eF}\ln\left(1-\frac{i}{2i_{L,c}}\right) \quad (30)$$

where $i_{L,a/c}$ denotes the limiting current density of the anode/cathode.

The terminal voltage of the SOFC can then be obtained from:

$$V = E - V_{act} - V_{ohm} - V_{conc} = E - \frac{RT}{n_eF}d_1 \quad (31)$$

where the expression of d_1 is given in Appendix.

4.1.3. Air blower

In order to overcome the pressure drop in the fuel cell stack as well as to drive the air through the system, a blower is needed in the SOFC sub-system to provide motive force to the incoming atmospheric air. The electrical power required to drive this component is typically one of the largest parasitic loads for the sub-system, and one that, if not carefully designed to meet the external power demand, can lower the overall system efficiency. A simple blower model is thus derived as follows to determine the power required:

$$P_{ab} = P_{fc}\eta_{ab} \quad (32)$$

where P_{ab} accounts for the parasitic electrical consumption in the air blower covered by the electricity generated by the SOFC, while η_{ab}, the power consumption factor, is defined as a ratio of the power provided by the SOFC itself for air blowing to the total amount of power generated by the SOFC, and its value is normally no more than 20% [37–39].

4.1.4. Combustor

Normally only part of the fuel can be oxidized in the fuel cell, an afterburner is thus required to combust the residual fuel and produce additional thermal energy for use elsewhere in the system. The role of the combustor in the micro-CHP is to burn non-reacted fuel coming out on the anode of the fuel cell with the non-reacted oxygen exiting the cathode. Based on the mass and energy balance of the combustor a model is developed to determine the flow-rate and temperature of the combustor exit stream, given known values for the inlet streams:

$$\dot{n}_{c-out}(H_2) = 0 \quad (33)$$

$$\dot{n}_{c-out}(CO) = 0 \quad (34)$$

$$\dot{n}_{c-out}(CO_2) = \dot{n}_{f-out}(CO_2) \quad (35)$$

$$\dot{n}_{c-out}(CH_4) = 0 \quad (36)$$

$$\dot{n}_{c-out}(H_2O) = \dot{n}_{f-out}(H_2O) + \dot{n}_{f-out}(H_2) \quad (37)$$

$$\dot{n}_{c-out}(N_2) = \dot{n}_{f-out}(N_2) + \dot{n}_{a-out}(N_2) \quad (38)$$

$$\dot{n}_{c-out}(O_2) = \dot{n}_{a-out}(O_2) - \frac{\dot{n}_{f-out}(H_2)}{2} \quad (39)$$

Given all flow-rates, the temperature of the combustor exit stream T_c can be further determined by solving the energy balance equation of the combustor:

$$\dot{H}_{f-out}(T_{f-out}) + \dot{H}_{a-out}(T_{a-out}) = \dot{H}_{c-out}(T_c) \quad (40)$$

where $T_{f-out} = T_{a-out} = T + \Delta T/2$. Eq. (40) implies that the exit temperature of the combustor T_c is a function of the SOFC operating temperature T.

4.1.5. Energy balance

Assuming ideal gas behaviour, the enthalpy of a stream can be calculated as a function of the molar flow rates and temperature by [30]:

$$\dot{H} = \sum_i \dot{n}_i h_i(T) = \sum_i \dot{n}_i\left(\Delta h_i^\circ + \int_{T_0}^{T} c_{p,i}\,dT\right) \quad (41)$$

where the molar enthalpy of each species i in the stream, $h_i(T)$, is given as a function of the local temperature, with Δh_i° being the standard enthalpy change of formation of species i ($J\,mol^{-1}$) and $c_{p,i}$ denoting the heat capacity of component i ($J\,mol^{-1}\,K^{-1}$).

The total enthalpy change for the SOFC section is therefore determined as:

$$\Delta\dot{H} = (-\Delta\dot{H}_{preheater}) + \Delta\dot{H}_{SOFC}$$
$$= \frac{iA}{n_eF}(-\Delta h_{preheater} + \Delta h_{SOFC}) = \frac{iA}{n_eF}\Delta h \quad (42)$$

where $\Delta\dot{H}_{preheater}$ represents the enthalpy change of the endothermic preheating process, and $\Delta\dot{H}_{SOFC}$ denotes the enthalpy change for the overall exothermic electrochemical reaction. $\Delta h = -\Delta h_{preheater} + \Delta h_{SOFC}$, where $\Delta h_{preheater}$ and Δh_{SOFC} are expressions given in Appendix.

The overpotential losses yield the rate of the total entropy production of the SOFC:

$$\dot{S}_{tot} = \frac{I(V_{act} + V_{ohm} + V_{conc})}{T_0} \quad (43)$$

where T_0 is the ambient temperature. Based on Eq. (43), the net power output of the SOFC is deduced as a function of current density, temperature, partial pressures, chemical composition, and geometric/material characteristics as:

$$P_{fc} = -\Delta\dot{G} - T_0S_{tot} - P_{ab} = \frac{iA(-\Delta g - RTd_1)}{n_eF(1+\eta_{ab})} \quad (44)$$

In terms of the efficiency, it is defined as the power output divided by the total energy input of the SOFC:

$$\eta_{fc} = \frac{P_{fc}}{-\Delta\dot{H}} = \frac{-\Delta_g - RTd_1}{-\Delta h(1+\eta_{ab})} \quad (45)$$

4.2. Modelling the heat exchangers

As illustrated in Fig. 4, two heat exchangers (HEX1 and HEX2) are adopted as pre-heaters to recycle the waste heat of the system and preheat the fuel cell incoming reactants in two steps, which are modelled as flat plate counter flow heat exchangers. According to Newtonian heat-transfer and the expression of log mean temperature difference (LMTD), the heat transfer rates for the counter-flow heat exchanger HEX1 and HEX2 can be expressed as:

$$\dot{Q}_{HEX1} = \dot{m}C_p(T_1 - T_0) = U_1A_1\frac{(T_3 - T_1) - (T_4 - T_0)}{\ln(((T_3 - T_1))/(T_4 - T_0))} \quad (46)$$

$$\dot{Q}_{HEX2} = \dot{m}C_p\left[\left(T - \frac{\Delta T}{2}\right) - T_1\right]$$
$$= U_2A_2\frac{[T_C - (T - (\Delta T/2))] - (T_3 - T_1)}{\ln((T_C - (T - (\Delta T/2)))/(T_3 - T_1))} \quad (47)$$

where $\dot{m}$ and C_p denote, respectively, the mass flow rate and heat capacity at constant pressure of the working fluid in the heat exchangers, U_1 and U_2 are the heat transfer coefficients of HEX1 and HEX2, A_1 and A_2 represent the corresponding heat transfer surface areas.

Comparison of Eq. (46) with Eq. (47) yields the following relation:

$$\frac{(T - (\Delta T/2)) - T_1}{T_1 - T_0} = b\frac{[T_C - (T - (\Delta T/2))] - (a-1)T_1}{(\alpha - 1)T - (T_4 - T_0)}$$
$$\cdot\frac{\ln(((a-1)T_1)/(T_4 - T_0))}{\ln(((T_C - (T - (\Delta T/2))))/((a-1)T_1))} \quad (48)$$

where $a = T_3/T_1$ and $b = (U_2A_2)/(U_1A_1)$ are two parameters representing temperature ratio and heat transfer performance of the two heat exchangers. Eq. (48) indicates that T_1 is a function of T_3 when other parameters are given.

Apart from heat exchangers, other irreversibilities such as heat loss from the SOFC directly to the environment cannot be neglected.

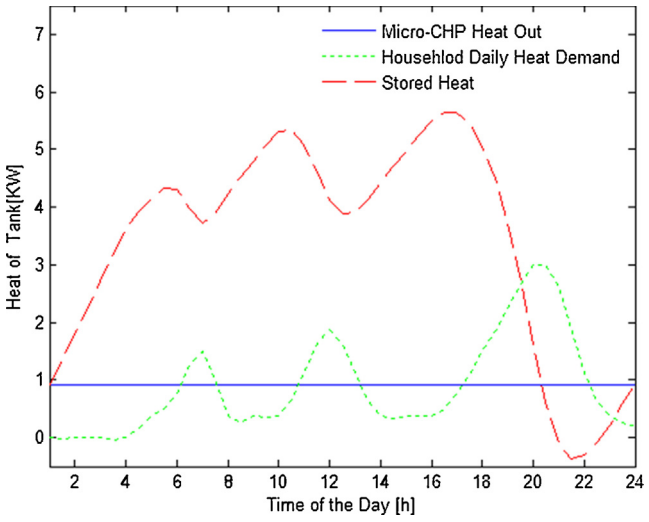

Fig. 5. Heat storage of the hot water tank.

In the present study, heat loss is modelled based on the temperature difference between the SOFC and ambient conditions [40–42]:

$$\dot{Q}_{loss} = KA_l(T - T_0) \quad (49)$$

where K denotes the effective convective and/or conductive heat-leak coefficient, and A_l represents the effective heat-transfer area. Note that this equation captures the effects of fuel cell temperature changes.

4.3. Modelling the hot water storage tank

Compared to electricity usage, large and rapid changes in domestic hot water usage are common. As the magnitude of these peaks can be reduced with thermal storage, a hot water tank is adopted in the micro-CHP system. Since the design volume of the tank depends on the peak heat demand rather than the average daily demand, a transient model that takes into account the changes of heat demand and supply over time is required. For simplicity, the content of the tank is assumed to be fully mixed, in which case the energy balance of the seasonal heat storage tank is expressed as follows:

$$M_{Tank}C_p\frac{dT}{dt} = \dot{Q}_{To-Tank} - \dot{Q}_{Demand}(T) \quad (50)$$

where C_p is the heat capacity of water, M_{Tank} denotes the mass of water contained in the tank, $\dot{Q}_{Demand}(T)$ is the amount of residential heat demand, and $\dot{Q}_{To-Tank}$ represents the heat supplied to the tank from the micro-CHP and the auxiliary boiler, which is assumed to be constant during the day and exactly match the residential daily heat demand [7].

The heat flow rates transferred from the SOFC to the water tank is obtained as follows:

$$\dot{Q}_{To-Tank} = \dot{Q}_{Heat} - \dot{Q}_{HEX1} - \dot{Q}_{HEX2} \quad (51)$$

where

$$\dot{Q}_{Heat} = -\Delta\dot{H} - P_{fc} - \dot{Q}_{loss} \quad (52)$$

and $\dot{Q}_{To-Tank}$ is calculated according to the expressions given in Appendix. Integration is used to calculate the temperature of the water storage tank, which is a function of time. Fig. 5 shows the performance of this heating system for a generic day, based on a SOFC micro-CHP with fully mixed storage tank. Since the tank

provides hot water at any time during the day, its volume is strongly related to the magnitude of the peak heat demand.

4.4. System efficiencies and heat-to-power ratio

Based on solution of Eqs. (44)–(52), the following expressions of the efficiencies for the micro-CHP system can be obtained:

Net electrical efficiency

$$\eta_{el,net} = \frac{P_{net}}{-\Delta\dot{H}} = \frac{P_{fc} - P_{parasitic}}{-\Delta\dot{H}} = \frac{P_{fc}(1-\eta_{ab})}{-\Delta\dot{H}} = \frac{1-\eta_{ab}}{\eta_{fc}} \quad (53)$$

Thermal efficiency

$$\eta_{thermal} = \frac{\dot{Q}_{Heat}}{-\Delta\dot{H}} \quad (54)$$

Total CHP efficiency

$$\eta_{CHP} = \frac{P_{net} + \dot{Q}_{heat}}{-\Delta\dot{H}} = \eta_{el,net} + \eta_{thermal} \quad (55)$$

System heat-to-power ratio

$$H2P = \frac{\dot{Q}_{Heat}}{P_{net}} \quad (56)$$

where P_{net} (W) denotes the DC power output of the SOFC, and $P_{parasitic}$ (W) is the electricity consumed internally in the system for power conditioning and the balance of plant.

5. Simulations and results

To determine the sensitivity of the overall system performance to the typical component parameters and to explore optimum system operation, numerical simulations of the micro-CHP system are carried out using MATLAB. The simulation model is based on a number of parameters which dramatically affect the results coming out from the MATLAB code. The model easily allows change and parameterization of any variable in it, such as SOFC current density, operating temperature, fuel utilization factor, etc., which are treated as independent design parameters that can individually be varied. The overall performance is thus predicted based on the validated data adopted from previous studies [5,38,43–45]. As summarized in Table 2, values of those parameters are used as constants throughout the study unless specifically mentioned.

5.1. The performance of the micro-CHP system

In order to investigate the ability of the micro-CHP system to meet the residential energy demand, selected system parameters were varied, and the sensitivity of the system performance to these parameters will be evaluated in the following sections.

First of all, the effect of the SOFC current density and operating temperature on the system performance of the micro-CHP is presented in Fig. 6. As shown in Fig. 6(a), the electrical efficiency of the micro-CHP system decreases with fuel cell current density, which implies an inherent benefit characteristic of all fuel cells, that the individual cell voltage rises when less current is drawn from it, giving a higher efficiency at lower load or part load. Specifically, the electrical efficiency drops sharply when the current density is higher than 7000 A/m^2, which is mainly due to the high polarization losses in the fuel cell. Moreover, the parasitic load will also decrease the electrical efficiency at low electrical load due to components that require constant electrical supply regardless of the power generated by the SOFC.

On the other hand, as plotted in Fig. 6(a), the electrical efficiency at higher current density, i.e., lower electrical load, will pass through a maximum value when the operating temperature of the

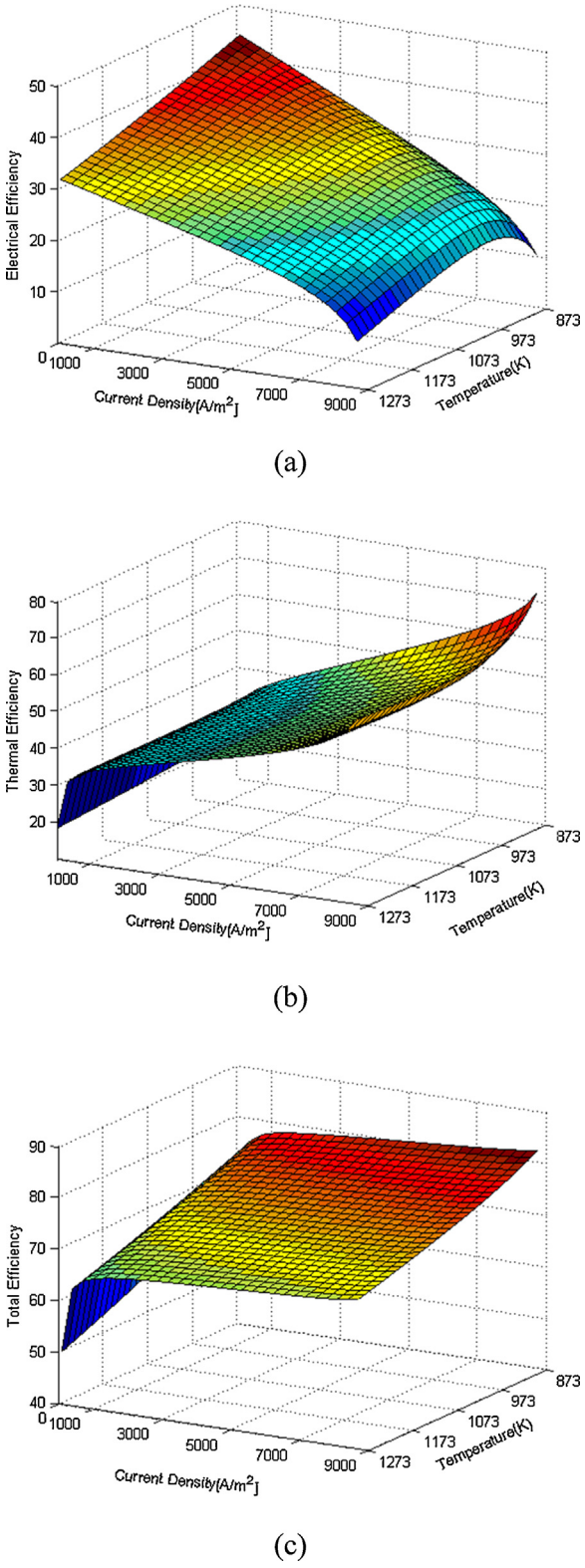

Fig. 6. The electrical efficiency (a), thermal efficiency (b) and total CHP efficiency (c) of the micro-CHP system varying with the operating temperature (T) and current density (i) of the SOFC.

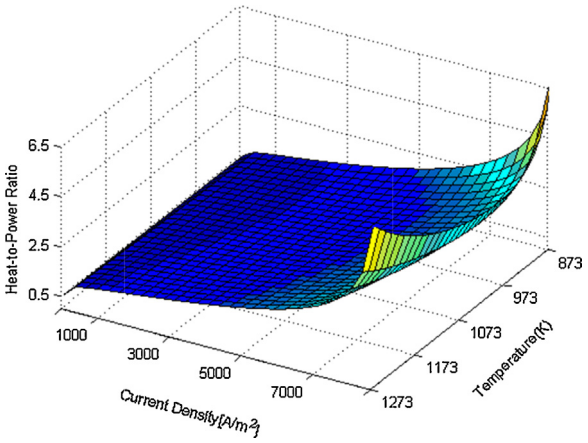

Fig. 7. Heat-to-power ratio of the micro-CHP system varying with the operating temperature (T) and current density (i) of the SOFC.

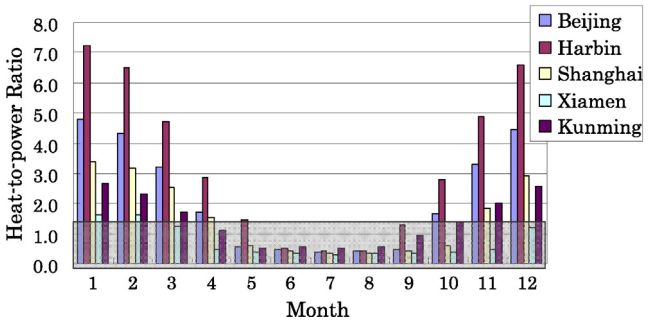

Fig. 8. Heat-to-power ratio of the residential energy demand during the year in five representative cities in China.

SOFC is increased from 873 K to 1073 K. This is mainly because the SOFC terminal voltage with respect to temperature rise has a peak instead of a monotonically changing trend, which means that a maximum value of the power density is achievable for a given current density, thereby leading to an optimal electrical efficiency as described in Fig. 6(a).

Fig. 6(b) depicts the sensitivity of the thermal efficiency of the micro-CHP system to the operating temperature and current density of the SOFC. As plotted in the figure, the thermal efficiency increases monotonically as the current density of the fuel cell is increased. At a higher current density, the thermal efficiency will increase dramatically as the electrical power output declines due to high polarization losses in the fuel cell, which can be further explained by Eqs. (44) and (51).

On the other hand, increasing the SOFC temperature tends to first decrease and then increase slightly the system thermal efficiency when the fuel cell is operated under a higher current density. This is due to many reasons. Firstly, increasing the SOFC temperature at a given current density leads to a greater amount of heat loss released to the environment according to Eq. (49). In addition, increasing the SOFC temperature also means an increase in the total energy input of the micro-CHP system. However, there exists a maximum value of the fuel cell power density when the temperature increases. According to Eqs. (52) and (54), this conclusively results in a first decreased and then increased optimal thermal efficiency as described in Fig. 6(b).

The total CHP efficiency of the SOFC micro-CHP system varying with the operating temperature and current density of the SOFC is plotted in Fig. 6(c). According to the simulation, the CHP efficiency decreases dramatically with increasing SOFC temperature, which is mainly due to the decreased electrical efficiency and thermal efficiency at a lower current density, as indicated by Eq. (55). On the contrary, the total CHP efficiency will increase monotonically with the SOFC current density. Specifically, the CHP efficiency increases sharply with current density when the electrical load is relatively high, mainly due to the significant increase in the electrical efficiency under higher electrical loads.

To illustrate how the SOFC temperature and current density affect the heat-to-power ratio of the micro-CHP system, Fig. 7 has been plotted and analyzed. The simulation results indicate that the system heat-to-power ratio will increase monotonically, from 0.5 to 6.5, with the current density of the SOFC, a characteristic that is beneficial during warm seasons when less heat is needed, with the extra benefit of an increase in the electrical efficiency as shown in Fig. 6(a). The effect of the SOFC operating temperature on the heat-to-power ratio can also be seen from Fig. 7, where the heat-to-power ratio will first decrease and then increase with an increasing temperature.

5.2. Optimal design of the micro-CHP system

Based on the energy demand profile presented in Fig. 3, the calculated heat-to-power ratio for a small family apartment is shown in Fig. 8. The area that is highlighted by a grey square represents the heat-to-power demand covered by the micro-CHP system without the use of an additional boiler. According to the analysis, the heat-to-power ratio range of the CHP system (approximately 0.5–2.5) under normal operating conditions shows a good agreement with the hot water and electricity demand of the residential apartments in different climate zones in China. However, when it is in cold climate regions where space heating is needed, the heat-to-power ratio of the household will increase significantly, reaching a value above 7, as depicted in Fig. 8. This implies that the heat-to-power ratio of the micro-CHP is not sufficient enough to cover the thermal energy demand over the whole year. For this reason, an auxiliary boiler and a hot water storage tank must be coupled with the micro-CHP. The challenge here is thus how to optimally design the micro-CHP system to accommodate the energy demand variances and mismatches.

During warm seasons, the heat-to-power ratios of the apartment and the micro-CHP are in a compatible range, i.e., around 0.5, as shown in Fig. 8. Therefore, to maximize its operating time and hence the economic and environmental benefit, the micro-CHP system should be sized according to the heat and electricity demand in warm seasons, and it should be operated in this period when there is limited heat demand.

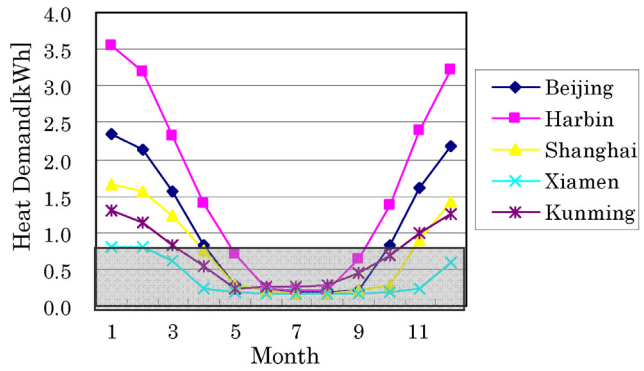

Fig. 9. Average daily residential thermal demand over the year in five representative cities in China.

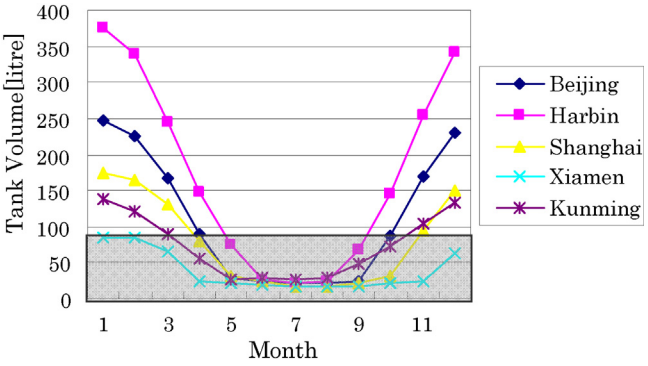

Fig. 10. Required volume of the hot water tank over the year in five representative cities in China.

During cold seasons, the winter heat demand needs to be taken into account when sizing the boiler. According to the average daily residential heat demand plotted in Fig. 9, cold seasons in China require up to 3.5 kWh of thermal energy for the use of space heating and hot water supply. The area highlighted by the grey square in Fig. 9 hence represents the heat demand that can be covered by the micro-CHP system.

When the micro-CHP is implemented in households where natural gas boilers are already installed, the hot water tank is still needed to recover and store the heat output of the micro-CHP when it is not needed. Typically this happens in warm seasons when electricity and hot water need to be supplied but space heating is not required. As the pre-existing boiler can already meet the overall thermal demand, the micro-CHP should be optimized in order to cope with the lowest heat-to-power ratio under the normal operating conditions. Additionally, the volume of the hot water tank needs to be optimized to cover the peak hot water demand of the residential apartment. The required volume of the water tank for each month that are calculated based on the heat demand data from Fig. 12 are plotted in Fig. 10, which indicates that the tank volume can be sized as approximately 80 l to ensure the operation of the micro-CHP during summer, according to the requirements in warm months. A larger volume will be required of course for the cold months, however since the auxiliary boiler can produce heat almost instantaneously, hot water supplied by the tank will not be needed. In terms of the auxiliary boiler, it should be sized to cover the large space heating demand in cold months, which obviously depends on the geographical location of the residence.

6. Conclusions

This work presents an investigation on the ability of a SOFC micro-CHP system to cover the heat and electricity demand of a 70 m^2 single-family household with an average number of occupants of 3. A detailed model for the micro-CHP system, which contains a SOFC coupled with a hot water storage tank and an auxiliary boiler, has been developed and analyzed. A transient model of the hot water storage tank is used to take into account the effect of peak residential heat demand. Numerical simulations are conducted in a Matlab environment. System design trade-offs are discussed to determine the optimal match between the energy demand of the household for different climates across China and the energy supply of the micro-CHP during the whole year. Moreover, criteria for sizing the system components of the micro-CHP are addressed specifically. The developed methodology can be applied to different types of residence with different load profiles.

Acknowledgments

The authors are grateful to the National Natural Science Foundation of China for support under grant No. 51206137. The work is also supported by Program for New Century Excellent Talents in University Grant No. NCET-11-0300.

Appendix.

1. The expression of d_1 in Eq. (31) is given as follows:

$$d_1 = 2\sinh^{-1}\left(\frac{i}{2i_{0,a}}\right) + 2\sinh^{-1}\left(\frac{i}{2i_{0,c}}\right) - \ln\left(1-\frac{i}{i_{L,a}}\right) - \ln\left(1-\frac{i}{i_{L,c}}\right) + \frac{in_eF}{RT}\left(\frac{L_e}{\sigma_e}+\frac{L_a}{\sigma_a}+\frac{L_c}{\sigma_c}+\frac{L_{\text{int}}}{\sigma_{\text{int}}}\right)$$

2. The expressions of $\Delta h_{preheater}$ and Δh_{SOFC} in Eq. (42) are given as follows:

$$\Delta h_{preheater} = \frac{[x_{H_2}h_{H_2}(T)+x_{CO}h_{CO}(T)+x_{CH_4}h_{CH_4}(T)+x_{CO_2}h_{CO_2}(T)+x_{N_2}h_{N_2}(T)+(2x_{CO}+4x_{CH_4})h_{H_2O}(T)]}{U_f x_{fc}} + \frac{[h_{O_2}(T)+3.7619h_{N_2}(T)]}{2U_a} - \frac{[x_{H_2}h_{H_2}(T_0)+x_{CO}h_{CO}(T_0)+x_{CH_4}h_{CH_4}(T_0)+x_{CO_2}h_{CO_2}(T_0)+x_{N_2}h_{N_2}(T_0)+(2x_{CO}+4x_{CH_4})h_{H_2O}(T_0)]}{U_f x_{fc}} - \frac{[h_{O_2}(T_0)+3.7619h_{N_2}(T_0)]}{2U_a}$$

$$\Delta h_{SOFC} = \frac{[(1-U_f)x_{fc}\cdot h_{H_2}(T)+(x_{CO}+x_{CO_2}+x_{CH_4})\cdot h_{CO_2}(T)+(x_{CO}+2x_{CH_4}+U_f x_{fc})\cdot h_{H_2O}(T)+x_{N_2}\cdot h_{N_2}(T)]}{U_f x_{fc}} + \frac{[(1-U_a)h_{O_2}(T)+3.7619h_{N_2}(T)]}{2U_a} - \frac{[x_{H_2}h_{H_2}(T)+x_{CO}h_{CO}(T)+x_{CH_4}h_{CH_4}(T)+x_{CO_2}h_{CO_2}(T)+x_{N_2}h_{N_2}(T)+(2x_{CO}+4x_{CH_4})h_{H_2O}(T)]}{U_f x_{fc}} - \frac{[h_{O_2}(T)+3.7619h_{N_2}(T)]}{2U_a}$$

References

[1] X. Gao, Y. Akashi, D. Sumiyoshi, Installed capacity optimization of distributed energy resource systems for residential buildings, Energy and Buildings 69 (2014) 307–317.
[2] M. Gandiglio, A. Lanzini, M. Santarelli, P. Leone, Design and optimization of a proton exchange membrane fuel cell CHP system for residential use, Energy and Buildings 69 (2014) 381–393.
[3] E.J. Naimaster Iv, A.K. Sleiti, Potential of SOFC CHP systems for energy-efficient commercial buildings, Energy and Buildings 61 (2013) 153–160.
[4] H. Lee, J. Bush, Y. Hwang, R. Radermacher, Modeling of micro-CHP (combined heat and power) unit and evaluation of system performance in building application in United States, Energy 58 (2013) 364–375.
[5] J. Larminie, A. Dicks, Fuel Cell Systems Explained, second ed., Wiley, England, 2003.
[6] Y. Zhao, J. Sadhukhan, A. Lanzini, N. Brandon, N. Shah, Optimal integration strategies for a syngas fuelled SOFC and gas turbine hybrid, Journal of Power Sources 196 (2011) 9516–9527.
[7] V. Liso, Y. Zhao, N. Brandon, M.P. Nielsen, S.K. Koer, Analysis of the impact of heat-to-power ratio for a SOFC-based mCHP system for residential application under different climate regions in Europe, International Journal of Hydrogen Energy 36 (2011) 13715–13726.
[8] E. Entchev, L. Yang, F. Szadkowski, M. Armstrong, M. Swinton, Application of hybrid micro-cogeneration system—thermal and power energy solutions for Canadian residences, Energy and Buildings 60 (2013) 345–354.

[9] A. Knizley, P.J. Mago, Evaluation of combined heat and power (CHP) systems performance with dual power generation units for different building configurations, International Journal of Energy Research 37 (2013) 1529–1538.
[10] V. Dorer, R. Weber, A. Weber, Performance assessment of fuel cell micro-cogeneration systems for residential buildings, Energy and Buildings 37 (2005) 1132–1146.
[11] H. Ren, W. Gao, Economic and environmental evaluation of micro CHP systems with different operating modes for residential buildings in Japan, Energy and Buildings 42 (2010) 853–861.
[12] A. Campos-Celador, E. Perez-Iribarren, J.M. Sala, L.A. del Portillo-Valdes, Thermoeconomic analysis of a micro-CHP installation in a tertiary sector building through dynamic simulation, Energy 45 (2012) 228–236.
[13] F. Zink, Y. Lu, L. Schaefer, A solid oxide fuel cell system for buildings, Energy Conversion and Management 48 (2007) 809–818.
[14] H. Xu, Z. Dang, B. Bai, Analysis of a 1 kW residential combined heating and power system based on solid oxide fuel cell, Applied Thermal Engineering 50 (2013) 1101–1110.
[15] A. Hawkes, I. Staffell, D. Brett, N. Brandon, Fuel cells for micro-combined heat and power generation, Energy and Environmental Science 2 (2009) 729–744.
[16] S.J.G. Cooper, G.P. Hammond, M.C. McManus, A. Ramallo-Gonzlez, J.G. Rogers, Effect of operating conditions on performance of domestic heating systems with heat pumps and fuel cell micro-cogeneration, Energy and Buildings 70 (2014) 52–60.
[17] G. Conroy, A. Duffy, L.M. Ayompe, Validated dynamic energy model for a Stirling engine μ-CHP unit using field trial data from a domestic dwelling, Energy and Buildings 62 (2013) 18–26.
[18] W. Feng, N. Zhou, C. Marnay, M. Stadler, J. Lai, Q. Liu, F. Rui, Building distributed energy performance optimization for China – a regional analysis of building energy costs and CO_2 emissions, in 2012 ACEEE summer study on energy efficiency in buildings, in: Asilomar Conference Center, Pacific Grove, CA, 2012.
[19] Ministry of Housing Ubran-Rural Development, Design Standard for Energy Efficiency of Residential Buildings in Severe Cold and Cold Zones – JGJ 26, Beijing, 2010.
[20] Ministry of Housing Ubran-Rural Development, Design Standard for Energy Efficiency of Residential Buildings in Hot Summer and Cold Winter Zone – JGJ 134, Beijing, 2010.
[21] Ministry of Housing Ubran-Rural Development, Design Standard for Energy Efficiency of Residential Buildings in Hot Summer Warm Winter Zone – JGJ 75, Beijing, 2003.
[22] Ministry of Housing Urban-Rural Development, Energy Conservation Design Standard for New Heating Residential Buildings – JGJ 26-95, Beijing, 1995.
[23] Ministry of Construction of the People's Republic of China, Climate Zones for Construction GB50178-93, China Planning Press, Beijing, 1994.
[24] Thematic Database for Human-earth System, 2013. http://www.data.ac.cn/
[25] Available from: http://www.tangent.com.cn/, 2013.
[26] China Statistical Database, 2013. http://219.235.129.58/welcome.do
[27] Building Energy Research Center of Tsinghua University, Annual Report on China Building Energy Efficiency, China Building Industry Press, Beijing, 2010.
[28] A. Martinez, K. Gerdes, R. Gemmen, J. Poston, Thermodynamic analysis of interactions between Ni-based solid oxide fuel cells (SOFC) anodes and trace species in a survey of coal syngas, Journal of Power Sources 195 (2010) 5206–5212.
[29] M. Granovskii, I. Dincer, M.A. Rosen, Performance comparison of two combined SOFC-gas turbine systems, Journal of Power Sources 165 (2007) 307–314.
[30] A.O. Omosun, A. Bauen, N.P. Brandon, C.S. Adjiman, D. Hart, Modelling system efficiencies and costs of two biomass-fuelled SOFC systems, Journal of Power Sources 131 (2004) 96–106.
[31] F. Calise, A. Palombo, L. Vanoli, Design and partial load exergy analysis of hybrid SOFC-GT power plant, Journal of Power Sources 158 (2006) 225–244.
[32] S.H. Chan, H.K. Ho, Y. Tian, Modelling for part-load operation of solid oxide fuel cell-gas turbine hybrid power plant, Journal of Power Sources 114 (2003) 213–227.
[33] B. Tarroja, F. Mueller, J. Maclay, J. Brouwer, Parametric thermodynamic analysis of a solid oxide fuel cell gas turbine system design space, Journal of Engineering for Gas Turbines and Power 132 (2010) 072301.
[34] C.O. Colpan, I. Dincer, F. Hamdullahpur, Thermodynamic modeling of direct internal reforming solid oxide fuel cells operating with syngas, International Journal of Hydrogen Energy 32 (2007) 787–795.
[35] F. Calise, G. Restucccia, N. Sammes, Experimental analysis of micro-tubular solid oxide fuel cell fed by hydrogen, Journal of Power Sources 195 (2010) 1163–1170.
[36] J. Sadhukhan, Y. Zhao, M. Leach, N.P. Brandon, N. Shah, Energy integration and analysis of solid oxide fuel cell based microcombined heat and power systems and other renewable systems using biomass waste derived syngas, Industrial and Engineering Chemistry Research 49 (2010) 11506–11516.
[37] R.T. Leah, N.P. Brandon, P. Aguiar, Modelling of cells, stacks and systems based around metal-supported planar IT-SOFC cells with CGO electrolytes operating at 500–600 °C, Journal of Power Sources 145 (2005) 336–352.
[38] E. Fontell, T. Kivisaari, N. Christiansen, J.B. Hansen, J. Pålsson, Conceptual study of a 250 kW planar SOFC system for CHP application, Journal of Power Sources 131 (2004) 49–56.
[39] S. Farhad, F. Hamdullahpur, Y. Yoo, Performance evaluation of different configurations of biogas-fuelled SOFC micro-CHP systems for residential applications, International Journal of Hydrogen Energy 35 (2010) 3758–3768.
[40] Y. Zhao, N. Shah, N. Brandon, The development and application of a novel optimization strategy for solid oxide fuel cell-gas turbine hybrid cycles, Fuel Cells 10 (2010) 181–193.
[41] Y. Zhao, N. Shah, N. Brandon, Comparison between two optimization strategies for solid oxide fuel cell-gas turbine hybrid cycles, International Journal of Hydrogen Energy 36 (2011) 10235–10246.
[42] D. Sánchez, A. Muñoz, T. Sánchez, An assessment on convective and radiative heat transfer modelling in tubular solid oxide fuel cells, Journal of Power Sources 169 (2007) 25–34.
[43] F. Mueller, R. Gaynor, A.E. Auld, J. Brouwer, F. Jabbari, G.S. Samuelsen, Synergistic integration of a gas turbine and solid oxide fuel cell for improved transient capability, Journal of Power Sources 176 (2008) 229–239.
[44] S.H. Chan, C.F. Low, O.L. Ding, Energy and exergy analysis of simple solid-oxide fuel-cell power systems, Journal of Power Sources 103 (2002) 188–200.
[45] J.P. Trembly, R.S. Gemmen, D.J. Bayless, The effect of IGFC warm gas cleanup system conditions on the gas–solid partitioning and form of trace species in coal syngas and their interactions with SOFC anodes, Journal of Power Sources 163 (2007) 986–996.